Solvent-Dependent Stabilization of Metastable Monolayer Polymorphs at the Liquid–Solid Interface

Thomas Sirtl,[†,‡] Wentao Song,[†,‡] Georg Eder,[†,‡] Subhadip Neogi,[§] Michael Schmittel,[§] Wolfgang M. Heckl,[†,‡,⊥] and Markus Lackinger[‡,⊥,*]

[†]Department of Physics, Technische Universität München, James-Franck-Str. 1, 85748 Garching, Germany, [‡]Center for NanoScience (CeNS), Schellingstr. 4, 80799 Munich, Germany, [§]Center of Micro- and Nanochemistry and Engineering, Organische Chemie I, Universität Siegen, Adolf-Reichwein-Str. 2, 57068 Siegen, Germany, and [⊥]Deutsches Museum, Museumsinsel 1, 80538 Munich, Germany

ABSTRACT Self-assembly of 1,3,5-tris(4′-biphenyl-4″-carbonitrile)benzene monolayers was studied at the liquid–solid interface by scanning tunneling microscopy. Application of different fatty acid homologues as solvents revealed a solvent-induced polymorphism. Yet, tempering triggered irreversible phase transitions of the initially self-assembled monolayers, thereby indicating their metastability. Interestingly, in either case, the same thermodynamically more stable and more densely packed monolayer polymorph was obtained after thermal treatment, irrespective of the initial structure. Again, the same densely packed structure was obtained in complementary solvent-free experiments conducted under ultrahigh vacuum conditions. Thus, self-assembly of metastable polymorphs at room temperature is explained by adsorption of partially solvated species under kinetic control. The irreversible phase transitions are induced by thermal desolvation, that is, desorption of coadsorbed solvent molecules.

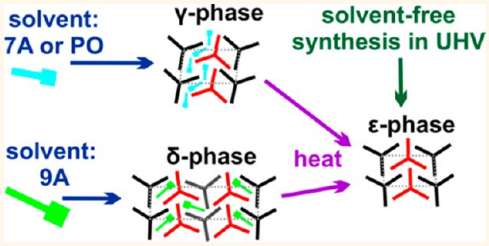

KEYWORDS: self-assembly · polymorphism · nitrile · phase transition · metastable · solvation · ultrahigh vacuum · liquid–solid · STM

Surface-supported self-assembled monolayers have been extensively studied over the past decade, due to their chemical and structural versatility, ranging from densely packed to porous two-dimensional structures.[1−3] Monolayer topologies are foremost determined by the chemical structure of the molecular building blocks, where type and stereochemical arrangement of functional groups decisively control intermolecular binding. However, the emergence of different monolayer polymorphs of a compound on the same surface already indicates an important influence of more subtle parameters, especially for self-assembly at the liquid–solid interface. Among those, solute concentration, temperature, and type of solvent were identified as being most important. In particular, solvent-induced polymorphism plays an important role because it is abundant, but its reasons are in most cases not clear.[4] For instance, a solvent-specific stabilization of certain monolayer structures is well-known for aromatic carboxylic acids,[5−10] foldable oligomers,[11] porphyrins,[12] or long-chain-substituted aromatic molecules.[13,14]

Different theoretical approaches such as Monte Carlo simulations,[15−18] molecular dynamics,[19] and thermodynamic models[20−24] were pursued to understand monolayer formation and selection processes. For the latter, it is assumed that the experimentally observed structures correspond to thermodynamic equilibrium. At the liquid–solid interface, this fundamental assumption is underpinned by experimental evidence for a dynamic equilibrium between dissolved and adsorbed molecules.[19,21] This phenomenon is unique for liquid–solid interfaces being the consequence of a drastically lowered desorption barrier due to solvation of the desorbed species in the supernatant liquid phase. An experimental manifestation of this dynamic equilibrium is the adaptation of the adsorbed monolayer structure to concentration changes in the liquid phase. For instance, transitions from a densely packed to a porous phase were observed for various compounds upon dilution.[8,20,23,25,26] Reversible temperature-driven phase transitions, likewise between a porous and a densely packed monolayer

* Address correspondence to markus@lackinger.org.

Received for review March 25, 2013 and accepted July 20, 2013.

Published online July 20, 2013
10.1021/nn4014577

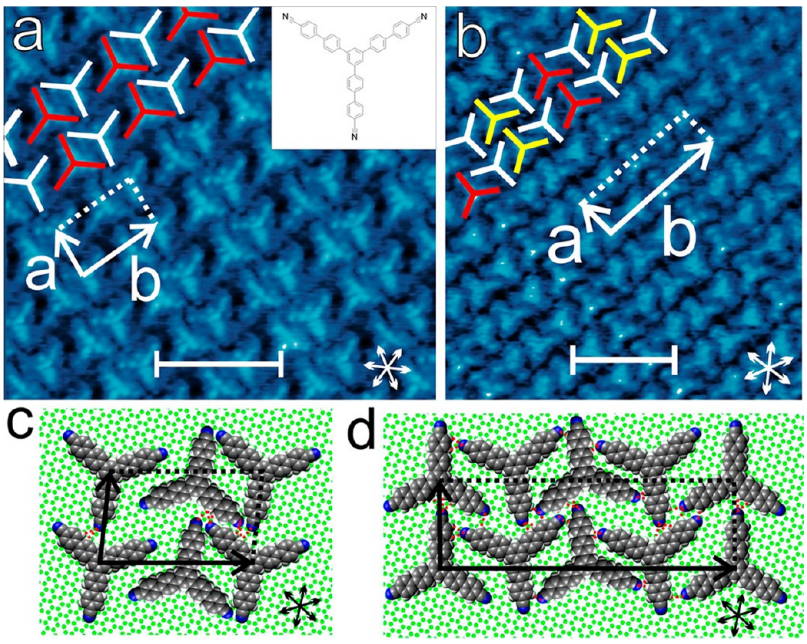

Figure 1. (a) STM image of the BCNB γ-phase at the heptanoic acid−graphite interface (56 pA, −0.35 V). Inset: Molecular structure of BCNB. (b) STM image of the BCNB δ-phase at the nonanoic acid−graphite interface (40 pA, −1.3 V). (c) Tentative model of the γ-phase. (d) Tentative model of the δ-phase. In (a) and (b), overlaid tripods symbolize BCNB molecules, and the unit cell vectors are denoted by arrows. Scale bars correspond to 5 nm. Arrows in the lower right corner indicate ⟨1000⟩ directions of graphite. The tentative models in (c) and (d) are based on the closest commensurate superstructures. DFT geometry-optimized BCNB molecules were used for the models and positioned according to the STM data (carbon atoms of BCNB, gray; carbon atoms of the graphite surface, green; hydrogen, white; nitrogen, blue). Conceivable intermolecular hydrogen bonds are indicated by dotted lines.

polymorph, provide further evidence for thermodynamical control.[24] Accordingly, thermodynamic models were successfully applied to understand structure selection in the concentration-dependent self-assembly of annulene, oligopyridine, and tricarboxylic acid monolayers[20,23,26,27] and the composition-dependent formation of binary tricarboxylic acid monolayers.[22]

Despite the utility of thermodynamical descriptions, counterexamples prove that an observed self-assembled monolayer structure does not necessarily represent a thermodynamically fully equilibrated situation.[19,21,25] In general, it remains difficult to experimentally decide whether a structure is the thermodynamically most favorable polymorph. A common method to disprove thermodynamic equilibrium is tempering, where irreversible phase transitions indicate conversion of metastable into equilibrium structures. For instance, upon heating of alkane-substituted hexabenzocoronene monolayers on Au(111), three subsequent phase transitions with a progressive increase in packing density were reported.[28] Similarly, thermally triggered irreversible phase transitions were observed in monolayers of polyaromatic molecules on graphite.[27,29] These findings are commonly explained by kinetic entrapment of the initial monolayer in a metastable state, and tempering provides the required activation energy for conversion into a thermodynamically more stable structure.

We present a study of monolayer self-assembly of the comparatively large polyaromatic trinitrile molecule 1,3,5-tris(4′-biphenyl-4″-carbonitrile)benzene (BCNB; see the inset to Figure 1a for molecular structure) at the liquid−solid interface, which targets the competition between kinetically and thermodynamically governed structure formation for larger compounds. By using fatty acid homologues as solvents, two different polymorphs were identified on graphite at room temperature. Yet, both polymorphs are irreversibly converted into the same, more densely packed monolayer by a thermal treatment, thereby indicating the metastability of both initial structures. In an attempt to unambiguously attribute this to solvent effects, complementary studies were carried out in a solution-free, utmost defined ultrahigh vacuum (UHV) environment.

RESULTS AND DISCUSSION

At the heptanoic acid−graphite interface, a self-assembled well-ordered BCNB monolayer termed γ-phase was observed. A representative STM image is shown in Figure 1a. From split images, lattice parameters of $a = 2.1 \pm 0.1$ nm, $b = 3.6 \pm 0.1$ nm, and $\gamma = 85 \pm 3°$ and an angle of $18 \pm 1°$ between the $\vec{a}$ vector of the superstructure and the graphite ⟨1000⟩ direction were determined. Within the experimental error, the BCNB lattice is consistent with a commensurate superstructure given by $\begin{pmatrix} 8 & -1 \\ 11 & 16 \end{pmatrix}$. Further evidence for commensurability is provided by the absence of a Moiré pattern as normally observed for incommensurate superstructures on graphite. BCNB adsorbs planarly and

each unit cell contains a pair of oppositely oriented molecules, as unambiguously concluded from the appearance of BCNB in the STM images. Adjacent molecules have similar orientation along $\vec{a}$, whereas they are alternatingly oriented along $\vec{b}$. Moreover, the nearest neighbor BCNB distances in this direction are alternating between ~1.5 nm and ~2.0 nm, allowing the dimers to be distinguished. Accordingly, the structure can be viewed as rows of stacked dimers running along $\vec{a}$ that are separated by small, but clearly recognizable, gaps. A tentative model of the BCNB dimer row structure is presented in Figure 1c. Owing to the large contact area between planarly adsorbed BCNB and graphite, the monolayer is to a large extent stabilized by molecule–substrate interactions. Additionally, the dimers bind through intermolecular C≡N···H–C hydrogen bonds, as indicated in Figure 1c. Formation of intermolecular hydrogen bonds was previously reported for BCNB on Ag(111) and Cu(111)[30] and is also well-known from other carbonitriles on surfaces[31−33] or in bulk crystals.[34,35] Further attractive electrostatic contributions might arise from so-called proton acceptor-ring interactions, as recently proposed in a theoretical *ab initio* study.[36] At this point, however, it remains unclear what causes and determines the spacing between the dimers.

At the nonanoic acid–graphite interface, a different and more complex BCNB monolayer polymorph termed δ-phase was observed. A representative STM image is depicted in Figure 1b, showing BCNB to be adsorbed in a planar fashion. Similar to the γ-phase, the orientation of adjacent BCNB molecules is equal along $\vec{a}$ and alternates along $\vec{b}$. Yet, along $\vec{b}$, the structure does not simply consist of equally spaced dimers, but exhibits a more complex stacking sequence that also comprises single molecules or trimers, again separated by small gaps. An example for the most frequently observed monomer–trimer–monomer sequence is depicted in Figure 1b. The corresponding unit cell contains four molecules and the underlying lattice parameters of $a = 2.0 \pm 0.1$ nm, $b = 6.7 \pm 0.3$ nm, and angle of $87 \pm 2°$ can again be mapped on a commensurate superstructure given by $\begin{pmatrix} 7 & -2 \\ 21 & 31 \end{pmatrix}$. A tentative model of the δ-phase is depicted in Figure 1d. Again, for the closely spaced BCNB molecules, stabilization by intermolecular C≡N···H–C hydrogen bonds is proposed. The BCNB nearest neighbor distances in a monomer–trimer–monomer sequence amount to ~1.9 nm ... ~1.6 nm ... ~1.6 nm ... ~1.8 nm. Thus, the intratrimer distance in the δ-phase (~1.6 nm) is similar to the intradimer distance in the γ-phase (~1.5 nm), and also the intertrimer (~1.8–1.9 nm) and interdimer (~2.0 nm) distances are comparable for the two phases. Occasionally, also more complex stacking sequences were observed for BCNB at the nonanoic acid–graphite interface, for instance, a monomer–dimer–monomer–dimer–monomer sequence, where the molecular orientation in successive monomer rows alternates (Figure 2). The corresponding unit cell containing six molecules is even larger with lattice parameters of $a = 2.1 \pm 0.2$ nm, $b = 9.7 \pm 0.6$ nm, and an angle of $89 \pm 4°$. Different stacking sequences can also occur within the same domain; an example is depicted in Figure 2b.

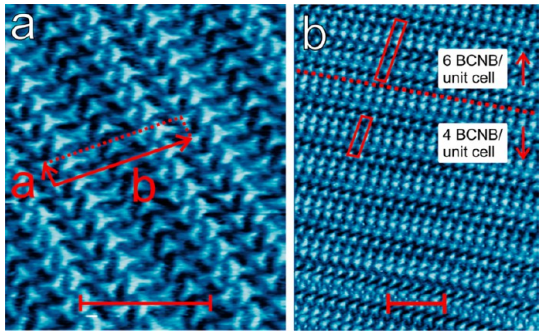

Figure 2. STM images of BCNB monolayers at the nonanoic acid–graphite interface. (a) Close-up of a variant of the δ-phase, exhibiting a monomer–dimer–monomer–dimer–monomer stacking sequence along $\vec{b}$. The unit cell vectors are indicated; $\vec{b}$ is elongated as compared to the most frequently observed δ-phase, and a unit cell contains six BCNB molecules (50 pA, −0.50 V). (b) Overview image depicting different stacking sequences within one domain of the δ-phase (65 pA, −1.2 V). Scale bars correspond to 10 nm.

Lattice parameters of all monolayer structures are summarized in Table 1. Interestingly, the spacing of similarly oriented molecules in rows parallel to $\vec{a}$ is quite similar for the γ-phase and the δ-phase, indicating a preferred distance between equally oriented stacked molecules and also a certain degree of analogy between these structures. Further experiments with pentanoic and octanoic acid as well as 1-phenyloctane (cf. Supporting Information) as solvents also yielded the γ-phase, rendering the δ-phase unique for nonanoic acid.

To explore whether the solvent-specific polymorphs represent the thermodynamically most favorable structures, experiments were conducted on thermally treated samples. For both polymorphs self-assembled at room temperature, thermal treatment at 70 °C for ~10 min results in irreversible phase transitions. Interestingly, irrespective of the initial structure, the same structure termed ε-phase emerges after tempering either the γ- or δ-phase. STM images of the ε-phase obtained from the two different initial structures are depicted in Figure 3b,c. Also tempering of the γ-phase prepared in 1-phenyloctane yielded the ε-phase (cf. Supporting Information). The ε-phase was characterized either by STM after *ex situ* heating and after the samples had cooled or additionally during *in situ* heating by STM imaging at an elevated temperature of 70 °C (in nonanoic acid, cf. Supporting Information) without finding any differences. The unit cells of all ε-phases obtained under different conditions are identical within experimental error.

The irreversible phase transitions clearly indicate the higher thermodynamic stability of the ε-phase, hence

TABLE 1. Lattice Parameters of All Experimentally Observed BCNB Monolayer Polymorphs

					surface packing density	
phase	*a* (nm)	*b* (nm)	∠*a,b*	∠*b,g*	(BCNB/nm^2)	(BCNB/unit cell)
γ	2.1 ± 0.1	3.6 ± 0.1	85 ± 3°	18 ± 1°	0.27 ± 0.02	2
γ^a	2.1[a]	3.5[a]	84°[a]	18°[a]	0.27[a]	2
δ	2.0 ± 0.1	6.7 ± 0.3	87 ± 2°	18 ± 2°	0.30 ± 0.02	4
δ^a	2.0[a]	6.7[a]	89°[a]	18°[a]	0.30[a]	4
δ^{ext}	2.1 ± 0.2	9.7 ± 0.6	89 ± 4°	19 ± 4°	0.29 ± 0.04	6
ε	2.0 ± 0.1	3.2 ± 0.1	88 ± 2°	20 ± 2°	0.31 ± 0.02	2
ε^{UHV}	1.9 ± 0.1	3.3 ± 0.1	82 ± 2°		0.32 ± 0.01	2
ε^a	1.9[a]	3.3[a]	86°[a]	19°[a]	0.32[a]	2

[a] Lattice parameters of the closest commensurate superstructures; *a* and *b*, absolute lengths of the unit cell vectors; ∠*a,b*, angle between *a* and *b*; ∠*b,g*, smallest angle between *b* and a graphite ⟨1000⟩ direction; δ^{ext}, additional variant of this phase with extended unit cell; ε^{UHV}, experimental results at the vacuum−graphite interface.

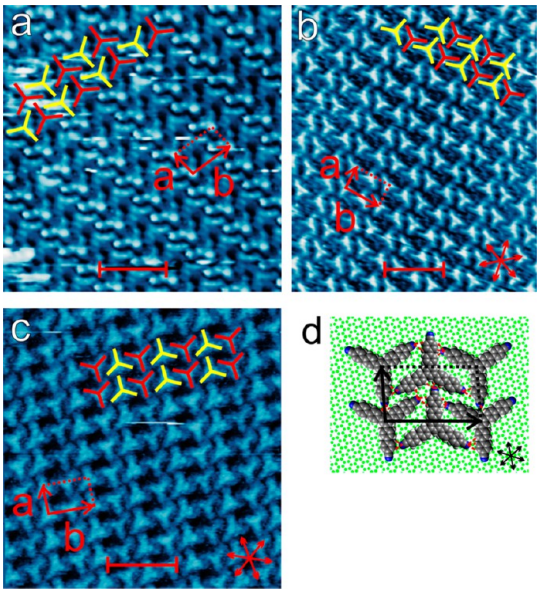

Figure 3. (a) STM image of the BCNB ε-phase at the vacuum−graphite interface (50 pA, +1.1 V). (b,c) STM images of *ex situ* tempered (70 °C; 10 min) samples with (b) nonanoic acid and (c) heptanoic acid: (b) 35 pA, −1.3 V; (c) 36 pA, −0.95 V. In both cases. the BCNB ε-phase was observed. (d) Tentative model of the ε-phase. Overlaid tripods in (a−c) indicate BCNB molecules, and the unit cell vectors *a* and *b* are marked. Scale bars correspond to 5 nm. Arrows denote ⟨1000⟩ directions of graphite.

the metastability of both γ- as well as δ-phase. A conversion of the metastable phases at room temperature without any additional thermal activation was never observed, not even in long-term experiments with prolonged exposure times of up to ∼1 week.

Lattice parameters of the ε-phase amount to 2.0 ± 0.1 nm, 3.2 ± 0.1 nm, and 88 ± 2° and are again consistently reproduced by a commensurate superstructure given by $\begin{pmatrix} 8 & 1 \\ 5 & 15 \end{pmatrix}$. BCNB molecules are again adsorbed planarly in the ε-phase, and the unit cell contains two molecules. Both the $\vec{a}$ lattice parameter and the orientation with respect to the graphite substrate are again comparable to the two metastable polymorphs. Similar to the γ- and δ-phases, adjacent BCNB molecules are oriented equally along $\vec{a}$ and alternatingly along $\vec{b}$. In contrast to the other phases, BCNB molecules are now evenly spaced with close proximity and the small gaps that were observed in the metastable polymorphs disappeared. BCNB nearest neighbor distances amount to ∼1.6−1.7 nm, comparable to the intradimer distance in the γ-phase (∼1.5 nm) and the intratrimer distances in the δ-phase (∼1.6 nm). This also leads to a smaller $\vec{b}$ lattice parameter of 3.3 nm in the ε-phase as compared to 3.5 nm of the γ-phase. Likewise, intermolecular C≡N···H−C hydrogen bonds contribute to the stabilization of the ε-phase. However, the closer packing and the absence of gaps implicate enhanced possibilities for intermolecular hydrogen bonds as compared to the room temperature phases. Accordingly, each of the nitrile groups in the ε-phase is involved in a stabilization of the structure *via* intermolecular hydrogen bonds.

Moreover, the ε-phase is the polymorph with the smallest unit cell, and thus features the highest surface packing density. A similar trend (*i.e.*, higher packing densities of the final structures) was commonly observed for irreversible phase transitions of surface-supported monolayers.[27−29] Decreased intermolecular distances offer an enthalpic advantage through stronger intermolecular bonds. Accordingly, in many cases, more densely packed monolayer polymorphs are thermodynamically more favorable.[19,21] Significant enthalpic contributions also arise from molecule−surface interactions that increase with packing density. Of course, structural changes that are associated with higher packing densities may also affect or even impair intermolecular bonds. However, the enthalpy change due to intermolecular bonds can be inferior in relation to the adsorption enthalpy, in particular, for large molecules. An instructive example therefore is the large tricarboxylic acid 1,3,5-tris(carboxybiphenyl)benzene, the monolayer structure of which is a compromise in favor of an increased packing density rather than optimized intermolecular hydrogen bonds.[26]

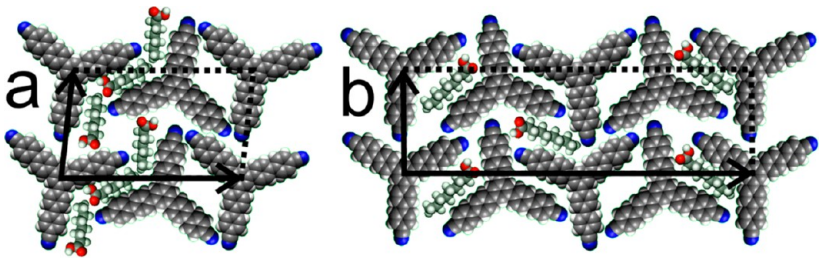

Figure 4. Tentative models for coadsorption of fatty acid solvent molecules in a hypothetical all-trans conformation. (a) Three heptanoic acid molecules per unit cell in the γ-phase. (b) Three nonanoic acid molecules per unit cell in the δ-phase. MM geometry-optimized molecular structures were used for solvents (carbon, gray; hydrogen, white; nitrogen, blue; oxygen, red). Unit cells are indicated by arrows and dashed lines.

We interpret the observed irreversible phase transitions from two distinct solvent-dependent monolayer polymorphs to a single solvent-independent structure as conversion of metastable polymorphs into thermodynamic equilibrium. Tempering provides the required energy to overcome the activation barrier. Additional experiments were carried out to substantiate the irreversibility of the phase transitions. If the phase transitions were reversible, γ- and δ-phases would be the thermodynamically preferred phases at room temperature. Accordingly, the ε-phase would only be observable at room temperature because it is kinetically trapped; that is, the rate of back-conversion is too slow. To support our hypothesis, graphite samples were immersed into solution, heated to 70 °C, and cooled at an extremely low rate of $\sim 6.2 \times 10^{-3}$ °C min^{-1} to facilitate a possible back-conversion. However, even with these extremely low cooling rates, the ε-phase prevailed, providing further indications that it actually is the thermodynamically more stable monolayer structure (cf. Supporting Information).

In the light of the many examples for solvent-induced polymorphism, it is remarkable that none of the initial room temperature polymorphs represents thermodynamic equilibrium. The solvent-dependent stabilization of different metastable polymorphs suggests a solvent-specific influence. One open question, however, is whether the solvent is the actual cause for the initial formation of metastable monolayer polymorphs. We address this intricate question by complementary experiments, where we study self-assembly of BCNB monolayers without any solvent in an utmost defined and clean environment. To this end, BCNB was deposited by thermal sublimation onto graphite under ultrahigh vacuum conditions and characterized *in situ* by STM. A representative STM image acquired at room temperature is shown in Figure 3a. Both lattice parameters and arrangement of BCNB are similar to the ε-phase observed at the liquid–solid interface. Based on the STM results and the equality of the unit cells, we conclude that vacuum deposition yields the same ε-phase as obtained from the thermally activated conversion of metastable γ- and δ-phases at the liquid–solid interface, respective images are shown in Figure 3b,c.

Apparently, the solvent directs the initial self-assembly toward metastable structures, giving rise to questions about the origin of this phenomenon. Given that both metastable phases are less densely packed than the stable ε-phase and exhibit gaps between otherwise densely packed rows of molecules, we propose that solvent coadsorption stabilizes both γ- and δ-phase. Solvent coadsorption is a well-known effect for self-assembly at the liquid–solid interface.[4] For instance, heptanoic acid solvent molecules were found to coadsorb in an upright geometry around coronene solute molecules on Au(111).[37] Their upright adsorption is mediated by strong interaction of the carboxyl groups with the metal substrate. On weakly interacting graphite surfaces, a different picture emerges: aliphatic solvent molecules as heptanol[38] or undecanol[39,40] were found to coadsorb planarly in an all-trans conformation in networks of isophthalic acid derivatives on graphite. For self-assembly of melamine structures in fatty acids, 12 solvent molecules bind radially to melamine hexamers by hydrogen bonds in an all-trans conformation, and the length of their alkane tails determines the lattice parameter.[41] Both the γ- and δ-phases provide enough void space for planarly adsorbed solvent molecules in the inter-row gaps, as illustrated in Figure 4a, where the uncovered area of the γ-phase can be filled with up to three heptanoic acid molecules per unit cell. An analogous tentative model for nonanoic acid coadsorption in the δ-phase is displayed in Figure 4b, where up to three nonanoic acid molecules can be coadsorbed in each unit cell. In the STM data, the solvent molecules cannot be clearly resolved, in accord with other studies.[5,10,24,42–48] Thus, no conclusions can be drawn on the precise adsorption geometry or conformation of the solvent molecules. Nevertheless, the tentative models clearly demonstrate that both metastable phases provide enough void space for solvent. On the other hand, the dense packing of the ε-phase does not facilitate solvent coadsorption, suggesting that it is a pure BCNB monolayer without any solvent contribution.

Solvation properties governed by the strength of interactions between solvents and solutes are discussed to be significant parameters for monolayer structure selection.[13,46,47] In solution, BCNB molecules

are solvated by fatty acid molecules with the strongest solvent–solute interaction arising from hydrogen bonding between carboxylic acid and nitrile groups. The similar observations realized with the nonprotic solvent 1-phenyloctane suggest that the type of solute–solvent interaction is not decisive. We propose that upon adsorption on graphite BCNB molecules only partially desolvate, so that the solvent molecules in the remaining solvation shell become likewise adsorbed on the surface. In this mixed solvent–solute adsorbate, the solvation shell prevents direct contact between adjacent BCNB molecules, thus giving rise to metastable polymers with the observed gaps between molecular rows. In the UHV experiments, that is, in the absence of solvent molecules, no solvation shell impedes close contact, and the thermodynamically more favorable ε-phase self-assembles directly.

Obviously, thermal energy at room temperature is not sufficient for a full desolvation of the adsorbed BCNB molecules, while higher temperatures initiate this irreversible entropy-driven process. Accordingly, the origin of this activation barrier is the favorable interaction of coadsorbed solvent molecules with both the graphite substrate and the stably adsorbed BCNB molecules. Once the solvent molecules have desorbed, the molecule–molecule interaction is increased by decreasing the mutual distance and thereby closing the inter-row gaps. A similar mechanism was proposed for coronene derivatives on Au(111), where solvent desorption already sets in at 25 °C.[28] The proposed straightforward mechanism for this desolvation-induced displacive phase transition is supported by the striking analogies between all polymorphs. Both the $\vec{a}$ lattice parameters and the orientation of the BCNB superstructures with respect to graphite are similar for all structures within experimental error. In addition, the relative orientations of adjacent molecules—equal along $\vec{a}$ and alternating along $\vec{b}$—are a common feature of all polymorphs. Consequently, the phase transition requires neither substantial structural changes as for instance the reorientation of molecules nor desorption or diffusion of BCNB molecules but is consistent with the model proposed above, where just the intermolecular gaps are closed by a comparatively small displacement of the molecules after complete desolvation.

The UHV experiments on graphite reveal remarkable differences to BCNB self-assembly on Ag(111) and Cu(111). On both metal surfaces, a trigonal, densely packed polymorph termed α-phase with one molecule per unit cell and almost similar lattice parameters of 1.80 and 1.77 nm was observed.[30] This structure appears ideal since its higher symmetry reflects the BCNB symmetry, and also, its packing density of 0.36 molecules/nm^2 is probably the highest achievable with planar adsorption. Accordingly, the different topology and the lower packing density of the ε-phase on graphite (0.32 molecules/nm^2) hints toward a substrate registry effect that would rather be expected for strongly interacting metal surfaces than for weakly interacting graphite.

CONCLUSION

At first sight, self-assembly of interfacial BCNB monolayers appears to be a further ordinary case of solvent-induced polymorphism. Despite its abundance, the origins of this phenomenon are in most cases not even qualitatively understood. On a fundamental level, it is often not clear whether different solvents affect the thermodynamical equilibrium or kinetically trap the system in a metastable state. By means of straightforward tempering experiments, we demonstrate that in the case of BCNB monolayers none of the initially self-assembled polymorphs corresponds to a fully thermodynamically controlled situation. For all different solvents, irreversible phase transitions lead to the same final monolayer, strongly suggesting that this is the thermodynamically most favorable polymorph. The two observed metastable polymorphs are less densely packed than the final structure due to small gaps between otherwise compact rows of monomers, dimers, or trimers. In principle, two possible reasons are conceivable for these in terms of molecule–molecule interactions' unfavorable gaps, either a substrate registry effect or solvent coadsorption. A clear distinction based on the STM data is not possible because the coadsorbed solvent molecules cannot be discerned. In order to nevertheless resolve this question, the studies at the liquid–solid interface were complemented by experiments in a solvent-free ultrahigh vacuum environment, where the same structure was found as after tempering the initial structures. From this, we conclude that self-assembly of the less densely packed polymorphs is not caused by substrate registry effects but by solvent coadsorption, even though clear signatures of solvent molecules were not identified in the STM data. Solvent coadsorption is attributed to incomplete desolvation when the BCNB molecules are adsorbed on graphite. Thus partially solvated BCNB molecules adsorb on the surface, preventing direct molecule–molecule contact. The energetic barrier for the desorption of solvent molecules (*i.e.*, full desolvation of the adsorbed BCNB molecules) cannot be overcome at room temperature, thus kinetically trapping metastable monolayer polymorphs.

On the basis of the present study, we conclude that even for highly dynamic self-assembly at the liquid–solid interface, the observed polymorph is not necessarily the thermodynamically most favorable structure. In particular, for less densely packed phases that are not obviously driven by the optimization of intermolecular bonding, simple *ex situ* tempering is an appropriate measure to reveal metastability of monolayer polymorphs. An important step toward

a fundamental understanding of self-assembly of surface-supported structures from liquids is to recognize and understand solvent effects. Here, we demonstrate that studying the same system in a solvent-free environment (*i.e.*, under UHV conditions) is a powerful combination.

MATERIALS AND METHODS

Synthesis details as well as the density functional theory optimized geometry of isolated BCNB (chemical abstract name: [1,1′:4′,1″:3″,1‴:4‴,1⁗-quinquephenyl]-4,4⁗-dicarbonitrile, 5″-(4′-cyano[1,1′-biphenyl]-4-yl)-) are reported elsewhere.[30] Molecular mechanics (MM) simulations were utilized for geometry optimization of fatty acid solvent molecules (Dreiding force field). BCNB monolayers were prepared on highly oriented pyrolytic graphite (HOPG, grade ZYB, Optigraph GmbH, Germany) both at the liquid−solid and the vacuum−solid interface and characterized by scanning tunneling microscopy (STM). All given tunneling voltages refer to the sample. STM topographs were drift corrected and processed by a mean value filter. STM experiments at the liquid−graphite interface were carried out with a home-built microscope operated by an ASC 500 control electronics (attocube Systems AG, Germany). Split images displaying both the adsorbate and graphite lattice within one frame were used for a precise determination of superstructure matrices.[49] Saturated solutions were prepared by mixing an excess of BCNB with 1 mL of the respective solvent (pentanoic acid, purity ≥99%; heptanoic acid, ≥ 97%; octanoic acid, ≥ 98%; nonanoic acid, ≥ 97%; 1-phenyloctane, ≥ 98%; all from Sigma-Aldrich), sonicating for 10 min, and subsequent centrifugation for 5 min. Samples were prepared by pipetting 5 μL of solution onto freshly cleaved HOPG. STM images were acquired with a mechanically cut Pt/Ir (90/10) tip immersed into the liquid. Samples were tempered at 70 °C either *in situ* with a home-built, resistively heated sample holder or *ex situ* in a preheated oven. During *in situ* heating, the temperature was measured at the bottom of the HOPG crystal with a thermocouple and controlled by a temperature controller (Eurotherm 2416, Invensys Inc., USA). STM images were acquired at elevated temperatures after thermal equilibration of the STM. *Ex situ* tempered samples were investigated after cooling. For both heating methods, the liquid phase was still present after tempering.

STM experiments at the vacuum−graphite interface were performed with a home-built beetle-type STM operated by an SPM-100 control electronics (RHK Technology Inc., USA). STM topographs were acquired with electrochemically etched tungsten tips at room temperature at a base pressure below 3×10^{-10} mbar. The HOPG crystal was prepared by electron-beam annealing at ~600 °C for several hours. Thoroughly outgassed BCNB was deposited from a home-built Knudsen cell at a crucible temperature of 340 °C.[50] A relatively slow monolayer deposition over 90 min promotes self-assembly of the thermodynamically most stable structure.

Conflict of Interest: The authors declare no competing financial interest.

Acknowledgment. We gratefully acknowledge financial support by the Nanosystems Initiative Munich (NIM) and the Fonds der Chemischen Industrie (FCI) (T.S.), as well as the Chinese Scholarship Council (W.S.), the Hanns-Seidel-Stiftung (G.E.), and the Alexander von Humboldt Stiftung (S.N.). We are indebted to Dr. Kingsuk Mahata for initial synthetic work.

Supporting Information Available: Additional STM data. This material is available free of charge *via* the Internet at http://pubs.acs.org.

REFERENCES AND NOTES

1. De Feyter, S.; de Schryver, F. C. Two-Dimensional Supramolecular Self-Assembly Probed by Scanning Tunneling Microscopy. *Chem. Soc. Rev.* **2003**, *32*, 139–150.
2. De Feyter, S.; de Schryver, F. C. Self-Assembly at the Liquid/Solid Interface: STM Reveals. *J. Phys. Chem. B* **2005**, *109*, 4290–4302.
3. Liang, H.; He, Y.; Ye, Y. C.; Xu, X. G.; Cheng, F.; Sun, W.; Shao, X.; Wang, Y. F.; Li, J. L.; Wu, K. Two-Dimensional Molecular Porous Networks Constructed by Surface Assembling. *Coord. Chem. Rev.* **2009**, *253*, 2959–2979.
4. Yang, Y.; Wang, C. Solvent Effects on Two-Dimensional Molecular Self-Assemblies Investigated by Using Scanning Tunneling Microscopy. *Curr. Opin. Colloid Interface Sci.* **2009**, *14*, 135–147.
5. Lackinger, M.; Griessl, S.; Heckl, W. M.; Hietschold, M.; Flynn, G. W. Self-Assembly of Trimesic Acid at the Liquid−Solid Interface—A Study of Solvent-Induced Polymorphism. *Langmuir* **2005**, *21*, 4984–4988.
6. Kampschulte, L.; Lackinger, M.; Maier, A.-K.; Kishore, R. S.; Griessl, S.; Schmittel, M.; Heckl, W. M. Solvent Induced Polymorphism in Supramolecular 1,3,5-Benzenetribenzoic Acid Monolayers. *J. Phys. Chem. B* **2006**, *110*, 10829–10836.
7. Ha, N. T. N.; Gopakumar, T. G.; Hietschold, M. Polymorphs of Trimesic Acid Controlled by Solvent Polarity and Concentration of Solute at Solid−Liquid Interface. *Surf. Sci.* **2013**, *607*, 68–73.
8. Florio, G. M.; Stiso, K. A.; Campanelli, J. S. Surface Patterning of Benzenecarboxylic Acids: Influence of Structure, Solvent, and Concentration on Molecular Self-Assembly. *J. Phys. Chem. C* **2012**, *116*, 18160–18174.
9. Zhang, X.; Chen, Q.; Deng, G. J.; Fan, Q. H.; Wan, L. J. Structural Diversity of a Monodendron Molecule Self-Assembly in Different Solvents Investigated by Scanning Tunneling Microscopy: From Dispersant to Counterpart. *J. Phys. Chem. C* **2009**, *113*, 16193–16198.
10. Li, Y. B.; Ma, Z.; Qi, G. C.; Yang, Y. L.; Zeng, Q. D.; Fan, X. L.; Wang, C.; Huang, W. Solvent Effects on Supramolecular Networks Formed by Racemic Star-Shaped Oligofluorene Studied by Scanning Tunneling Microscopy. *J. Phys. Chem. C* **2008**, *112*, 8649–8653.
11. Shen, Y. T.; Zhu, N. B.; Zhang, X. M.; Deng, K.; Feng, W.; Yan, Q. F.; Lei, S. B.; Zhao, D. H.; Zeng, Q. D.; Wang, C. A Foldamer at the Liquid/Graphite Interface: The Effect of Interfacial Interactions, Solvent, Concentration, and Temperature. *Chem.—Eur. J.* **2011**, *17*, 7061–7068.
12. Takami, T.; Mazur, U.; Hipps, K. W. Solvent-Induced Variations in Surface Structure of a 2,9,16,23-Tetra-*tert*-butylphthalocyanine on Graphite. *J. Phys. Chem. C* **2009**, *113*, 17479–17483.
13. Miao, X.; Xu, L.; Li, Z.; Deng, W. Solvent-Induced Structural Transitions of a 1,3,5-Tris(10-ethoxycarbonyldecyloxy)-benzene Assembly Revealed by Scanning Tunneling Microscopy. *J. Phys. Chem. C* **2011**, *115*, 3358–3367.
14. Xu, L.; Miao, X. R.; Zha, B.; Deng, W. L. Self-Assembly Polymorphism: Solvent-Responsive Two-Dimensional Morphologies of 2,7-Ditridecyloxy-9-fluorenone by Scanning Tunneling Microscopy. *J. Phys. Chem. C* **2012**, *116*, 16014–16022.
15. Weber, U. K.; Burlakov, V. M.; Perdigao, L. M. A.; Fawcett, R. H. J.; Beton, P. H.; Champness, N. R.; Jefferson, J. H.; Briggs, G. A. D.; Pettifor, D. G. Role of Interaction Anisotropy in the Formation and Stability of Molecular Templates. *Phys. Rev. Lett.* **2008**, *100*, 156101.
16. Martsinovich, N.; Troisi, A. Modeling the Self-Assembly of Benzenedicarboxylic Acids Using Monte Carlo and Molecular Dynamics Simulations. *J. Phys. Chem. C* **2010**, *114*, 4376–4388.
17. Adisoejoso, J.; Tahara, K.; Lei, S.; Szabelski, P.; Rzysko, W.; Inukai, K.; Blunt, M. O.; Tobe, Y.; De Feyter, S. One Building Block, Two Different Nanoporous Self-Assembled Monolayers: A Combined STM and Monte Carlo Study. *ACS Nano* **2012**, *6*, 897–903.

18. Lei, S.; Tahara, K.; Müllen, K.; Szabelski, P.; Tobe, Y.; De Feyter, S. Mixing Behavior of Alkoxylated Dehydrobenzo-[12]Annulenes at the Solid−Liquid Interface: Scanning Tunneling Microscopy and Monte Carlo Simulations. *ACS Nano* **2011**, *5*, 4145–4157.
19. Uemura, S.; Tanoue, R.; Yilmaz, N.; Ohira, A.; Kunitake, M. Molecular Dynamics in Two-Dimensional Supramolecular Systems Observed by STM. *Materials* **2010**, *3*, 4252–4276.
20. Lei, S.; Tahara, K.; de Schryver, F. C.; van der Auweraer, M.; Tobe, Y.; De Feyter, S. One Building Block, Two Different Supramolecular Surface-Confined Patterns: Concentration in Control at the Solid−Liquid Interface. *Angew. Chem., Int. Ed.* **2008**, *47*, 2964–2968.
21. Gutzler, R.; Cardenas, L.; Rosei, F. Kinetics and Thermodynamics in Surface-Confined Molecular Self-Assembly. *Chem. Sci.* **2011**, *2*, 2290–2300.
22. Kampschulte, L.; Werblowsky, T. L.; Kishore, R. S. K.; Schmittel, M.; Heckl, W. M.; Lackinger, M. Thermodynamical Equilibrium of Binary Supramolecular Networks at the Liquid−Solid Interface. *J. Am. Chem. Soc.* **2008**, *130*, 8502–8507.
23. Meier, C.; Roos, M.; Künzel, D.; Breitruck, A.; Hoster, H. E.; Landfester, K.; Gross, A.; Behm, R. J.; Ziener, U. Concentration and Coverage Dependent Adlayer Structures: From Two-Dimensional Networks to Rotation in a Bearing. *J. Phys. Chem. C* **2010**, *114*, 1268–1277.
24. Gutzler, R.; Sirtl, T.; Dienstmaier, J. F.; Mahata, K.; Heckl, W. M.; Schmittel, M.; Lackinger, M. Reversible Phase Transitions in Self-Assembled Monolayers at the Liquid−Solid Interface: Temperature-Controlled Opening and Closing of Nanopores. *J. Am. Chem. Soc.* **2010**, *132*, 5084–5090.
25. Jahanbekam, A.; Vorpahl, S.; Mazur, U.; Hipps, K. W. Temperature Stability of Three Commensurate Surface Structures of Coronene Adsorbed on Au(111) from Heptanoic Acid in the 0 to 60 °C Range. *J. Phys. Chem. C* **2013**, *117*, 2914–2919.
26. Dienstmaier, J. F.; Mahata, K.; Walch, H.; Heckl, W. M.; Schmittel, M.; Lackinger, M. On the Scalability of Supramolecular Networks—High Packing Density *vs* Optimized Hydrogen Bonds in Tricarboxylic Acid Monolayers. *Langmuir* **2010**, *26*, 10708–10716.
27. Bellec, A.; Arrigoni, C.; Schull, G.; Douillard, L.; Debuisschert, C. F.; Mathevet, F.; Kreher, D.; Attias, A. J.; Charra, F. Solution-Growth Kinetics and Thermodynamics of Nanoporous Self-Assembled Molecular Monolayers. *J. Chem. Phys.* **2010**, *134*, 124702.
28. Marie, C.; Silly, F.; Tortech, L.; Müllen, K.; Fichou, D. Tuning the Packing Density of 2D Supramolecular Self-Assemblies at the Solid−Liquid Interface Using Variable Temperature. *ACS Nano* **2010**, *4*, 1288–1292.
29. Li, Y. B.; Liu, C. H.; Xie, Y. Z.; Li, X. K.; Li, X.; Fan, X. L.; Deng, K.; Zeng, Q. D.; Wang, C. Temperature-Controlled Self-Assembling Structure with Selective Guest-Recognition at the Liquid−Solid Interface. *Phys. Chem. Chem. Phys.* **2013**, *15*, 125–128.
30. Sirtl, T.; Schlögl, S.; Rastgoo-Lahrood, A.; Jelic, J.; Neogi, S.; Schmittel, M.; Heckl, W. M.; Reuter, K.; Lackinger, M. Control of Intermolecular Bonds by Deposition Rates at Room Temperature: Hydrogen Bonds *versus* Metal Coordination in Trinitrile Monolayers. *J. Am. Chem. Soc.* **2013**, *135*, 691–695.
31. Yokoyama, T.; Yokoyama, S.; Kamikado, T.; Okuno, Y.; Mashiko, S. Selective Assembly on a Surface of Supramolecular Aggregates with Controlled Size and Shape. *Nature* **2001**, *413*, 619–621.
32. Pawin, G.; Wong, K. L.; Kim, D.; Sun, D. Z.; Bartels, L.; Hong, S.; Rahman, T. S.; Carp, R.; Marsella, M. A Surface Coordination Network Based on Substrate-Derived Metal Adatoms with Local Charge Excess. *Angew. Chem., Int. Ed.* **2008**, *47*, 8442–8445.
33. Kühne, D.; Klappenberger, F.; Decker, R.; Schlickum, U.; Brune, H.; Klyatskaya, S.; Ruben, M.; Barth, J. V. Self-Assembly of Nanoporous Chiral Networks with Varying Symmetry from Sexiphenyl-Dicarbonitrile on Ag(111). *J. Phys. Chem. C* **2009**, *113*, 17851–17859.
34. Özbey, S.; Kaynak, F. B.; Göker, H.; Kus, C. Synthesis and Crystal Structure Elucidation of 1-(4-Fluorobenzyl)-2-(4-cyanophenyl)-1*H*-benzimidazole-5-carbonitrile. *J. Chem. Crystallogr.* **2004**, *34*, 851–858.
35. Döpp, D.; Kruse, C.; Flörke, U.; Henkel, G. Rel-(1r,4r,9r)-1-Acetyl-9-(1-Pyrrolidinyl)-1,4-dihydro-1,4-ethanonaphthalene-9-carbonitrile: The Major [4 + 2]-Photocycloadduct of 1-Acetonaphthone with 2-(1-Pyrrolidinyl) Propenenitrile. *Acta Crystallogr., Sect. E* **2006**, *62*, O3245–O3246.
36. Arras, E.; Seitsonen, A. P.; Klappenberger, F.; Barth, J. V. Nature of the Attractive Interaction between Proton Acceptors and Organic Ring Systems. *Phys. Chem. Chem. Phys.* **2012**, *14*, 15995–16001.
37. Gyarfas, B. J.; Wiggins, B.; Zosel, M.; Hipps, K. W. Supramolecular Structures of Coronene and Alkane Acids at the Au(111)-Solution Interface: A Scanning Tunneling Microscopy Study. *Langmuir* **2005**, *21*, 919–923.
38. De Feyter, S.; Grim, P. C. M.; Rucker, M.; Vanoppen, P.; Meiners, C.; Sieffert, M.; Valiyaveettil, S.; Müllen, K.; de Schryver, F. C. Expression of Chirality by Achiral Coadsorbed Molecules in Chiral Monolayers Observed by STM. *Angew. Chem., Int. Ed.* **1998**, *37*, 1223–1226.
39. Vanoppen, P.; Grim, P. C. M.; Rucker, M.; DeFeyter, S.; Moessner, G.; Valiyaveettil, S.; Mullen, K.; DeSchryver, F. C. Solvent Codeposition and cis-trans Isomerization of Isophthalic Acid Derivatives Studied by STM. *J. Phys. Chem.* **1996**, *100*, 19636–19641.
40. Grim, P. C. M.; Vanoppen, P.; Rucker, M.; DeFeyter, S.; Valiyaveettil, S.; Moessner, G.; Müllen, K.; DeSchryver, F. C. Molecular Organization of Azobenzene Derivatives at the Liquid/Graphite Interface Observed with Scanning Tunneling Microscopy. *J. Vac. Sci. Technol., B* **1997**, *15*, 1419–1424.
41. Walch, H.; Maier, A. K.; Heckl, W. M.; Lackinger, M. Isotopological Supramolecular Networks from Melamine and Fatty Acids. *J. Phys. Chem. C* **2009**, *113*, 1014–1019.
42. Saiz-Poseu, J.; Martinez-Otero, A.; Roussel, T.; Hui, J. K. H.; Montero, M. L.; Urcuyo, R.; MacLachlan, M. J.; Faraudo, J.; Ruiz-Molina, D. Self-Assembly of a Catechol-Based Macrocycle at the Liquid−Solid Interface: Experiments and Molecular Dynamics Simulations. *Phys. Chem. Chem. Phys.* **2012**, *14*, 11937–11943.
43. Kikkawa, Y.; Kihara, H.; Takahashi, M.; Kanesato, M.; Balaban, T. S.; Lehn, J. M. Two-Dimensional Structures of Anthracene Derivatives: Photodimerization and Host−Guest Chemistry. *J. Phys. Chem. B* **2010**, *114*, 16718–16722.
44. Kikkawa, Y.; Omori, K.; Kanesato, M.; Hiratani, K. Two-Dimensional Structures of Isobutenyl Ether Compounds Possessing Dodecyl and Tridecyl Chains: Effects of Solvent and Tandem Claisen Rearrangement. *Chem. Lett.* **2012**, *41*, 1196–1198.
45. Ma, Z.; Wang, Y. Y.; Wang, P.; Huang, W.; Li, Y. B.; Lei, S. B.; Yang, Y. L.; Fan, X. L.; Wang, C. Star-Shaped Oligofluorenes End-Capped with Carboxylic Groups: Syntheses and Self-Assembly at the Liquid−Solid Interface. *ACS Nano* **2007**, *1*, 160–167.
46. Mamdouh, W.; Uji-i, H.; Ladislaw, J. S.; Dulcey, A. E.; Percec, V.; de Schryver, F. C.; De Feyter, S. Solvent Controlled Self-Assembly at the Liquid−Solid Interface Revealed by STM. *J. Am. Chem. Soc.* **2006**, *128*, 317–325.
47. Tahara, K.; Furukawa, S.; Uji-i, H.; Uchino, T.; Ichikawa, T.; Zhang, J.; Mamdouh, W.; Sonoda, M.; de Schryver, F. C.; De Feyter, S.; *et al.* Two-Dimensional Porous Molecular Networks of Dehydrobenzo[12]annulene Derivatives *via* Alkyl Chain Interdigitation. *J. Am. Chem. Soc.* **2006**, *128*, 16613–16625.
48. Lee, S. Y.; Noh, J.; Ito, E.; Lee, H.; Hara, M. Solvent Effect on Formation of Cysteamine Self-Assembled Monolayers on Au(111). *Jpn. J. Appl. Phys., Part 1* **2003**, *42*, 236–241.
49. Lackinger, M.; Heckl, W. M. Carboxylic Acids: Versatile Building Blocks and Mediators for Two-Dimensional Supramolecular Self-Assembly. *Langmuir* **2009**, *25*, 11307–11321.
50. Gutzler, R.; Heckl, W. M.; Lackinger, M. Combination of a Knudsen Effusion Cell with a Quartz Crystal Microbalance: *In Situ* Measurement of Molecular Evaporation Rates with a Fully Functional Deposition Source. *Rev. Sci. Instrum.* **2010**, *81*, 015108.